Journal of Sound and Vibration 589 (2024) 118540

Contents lists available at ScienceDirect

Journal of Sound and Vibration

journal homepage: www.elsevier.com/locate/jsvi

An enhanced indirect modal identification procedure for bridges based on the dynamic response of moving vehicles

Matteo Mazzeo [a], Alberto Di Matteo [b,*], Roberta Santoro [a]

[a] *Department of Engineering, University of Messina, Contrada Di Dio, 98166 Sant'Agata, Messina, Italy*
[b] *Department of Engineering, University of Palermo, Viale delle Scienze, 90128, Palermo, Italy*

ARTICLE INFO

Keywords:
Indirect health monitoring
Vehicle scanning method
Vehicle–bridge interaction
Variational mode decomposition
Damping identification
Mode shapes estimation

ABSTRACT

Indirect dynamic structural identification, referred to as Vehicle Scanning Method (VSM), pertains to the estimation of bridge modal parameters by using data recorded from sensors directly mounted on a moving vehicle. This procedure has recently gained increasing attention due to its low cost and simple implementation. Nevertheless, the non-stationary and complex nature of the vehicle–bridge interaction phenomenon poses some limitations to the applicability of the method, especially in terms of accuracy. In this regard, in this paper, an enhanced procedure for the dynamic identification of bridges modal parameters based on the VSM is introduced, taking into account the effects of vehicle/bridge damping and road pavement roughness. Specifically, based on the Variational Mode Decomposition (VMD) method, the relevant Intrinsic Mode Functions (IMFs) and corresponding modal frequencies are determined from the recorded signal. Further, the Natural Excitation Technique (NExT) is adopted in conjunction with a noise-robust area ratio-based approach, for modal damping ratios estimation. Finally, mode shapes are evaluated by properly correcting the instantaneous amplitudes of each IMF considering the influence of the corresponding estimated modal damping ratio. Several numerical simulations are presented to show the validity of the proposed procedure and comparisons with the classical Hilbert Spectrum-based identification approach are employed to assess its reliability and improved accuracy.

1. Introduction

In the last decades, the development of vibration-based techniques for structural identification has become a relevant area among researchers in the civil and mechanical engineering community, especially for structural health monitoring (SHM) purposes [1]. Vibration-based testing relies on the concept that structural modal parameters depend on several physical characteristics of the structure and change when deterioration or damaging mechanism occurs [2]. Notably, classical direct monitoring approaches typically require permanent placement of a large network of sensors on the structure. In this manner, the recorded responses due to ambient excitation are processed, and classic methods of Operational Modal Analysis (OMA) are used to estimate the modal parameters. However, due to the large number of sensors generally required for each structure, this strategy is not always feasible. Direct vibration monitoring becomes uneconomical particularly for medium or short-span bridges thus limiting its application only to specific critical infrastructures. In this regard, significant limitations of the direct monitoring approach include the high installation and maintenance costs, the conspicuous volume of raw data to be processed, and the different durability timespan between the monitored structure and monitoring system [3].

* Corresponding author.
E-mail address: alberto.dimatteo@unipa.it (A. Di Matteo).

https://doi.org/10.1016/j.jsv.2024.118540
Received 3 October 2023; Received in revised form 12 April 2024; Accepted 27 May 2024
Available online 28 May 2024

On this basis, several research efforts have been focused on the development of different and more economical vibration-based procedures that may lead to the assessment of the condition of a large number of bridges. In this framework, an indirect approach generally referred to as vehicle scanning method (VSM) has recently gained increasing attention among researchers in the field, due to its ability to possibly overcome classical direct approach main limitations. This procedure, firstly introduced by Yang et al. [4,5], is based on a drive-by approach where a testing vehicle (modeled as a simplified mass–spring–damper system) moves over the bridge, while its vertical acceleration response is recorded via few sensors directly mounted on the car body or its axle. Further, Yang et al. [6] recently proposed a closed-form solution for the vehicle–bridge dynamic response in the more general case of a two-axle asymmetric vehicle.

Notably, although both lab-scaled models [7] and in situ testing [8–11] have shown the validity of the VSM in estimating the fundamental frequency of the bridge, some issues may arise when dealing with this procedure. Generally, for instance, the recorded response is affected by the vehicle-related frequency content. In this case, the associated frequency spectrum usually shows a peak related to the vehicle's natural frequency whose magnitude may be significantly higher than the structural ones, thus making it difficult to identify the bridge frequencies. To cope with this issue, the use of the acceleration response at the contact point between the vehicle tyre and the surface has been suggested [12].

Further, the effect of the pavement roughness poses additional challenges on the accuracy of the estimated parameters, since the introduced high-frequency noise components can overshadow higher modes frequencies. To address this issue, a possible strategy relates to the use of the residual signal from the measurements of two connected vehicles [13] or the vehicle front and rear tyre [14,15]. Alternatively, advanced decomposition techniques can be employed to separate the modal components from the noise produced by road pavement.

In this regard, one of the most adopted methods is the Empirical Mode Decomposition (EMD) [16] which employs an iterative sifting process to extract modal components, generally referred to as Intrinsic Mode Functions (IMFs). This method, however, may suffer from mode mixing problems and improved versions of the EMD such as Ensemble Empirical Mode Decomposition (EEMD) [17] have been successively proposed. In the context of VSM-based monitoring, in [18] the EMD has been used in combination with Fourier transform to estimate the bridge frequencies from data of a passing vehicle, whereas in [19] an EMD-based damage index has been proposed to assess the bridge health condition. Further, in [20,21] EEMD has been applied to obtain improved bridge modal parameters estimations from drive-by measurements also capturing sudden stiffness changes.

In the last decades, however, several other decomposition techniques have been proposed and applied for SHM purposes, among which the Variational Mode Decomposition (VMD) [22] has proved to achieve high decomposition quality in standard direct bridges dynamic identification procedures [23,24]. This method is based on a variational formulation that yields an adaptive extraction of relevant modal components from a given time series and their corresponding central frequencies (also referred to as dominant frequencies).

Notably, the applicability of VMD to the field of indirect dynamic identification has been analyzed to a lesser degree. For instance, in [25] both numerical and experimental studies have assessed the efficiency of the VMD for the modal frequencies estimations and no mode mixing effects have been observed. Further, Yang et al. [26] presented a theoretical procedure for the estimation of the vertical and lateral mode shapes of a curved bridge from a single-axle test vehicle combining VMD and synchrosqueezed wavelet transform technique. Similarly, in [27] an approach has been proposed that combines the zero-phase filtering decomposition technique with a three-step correction procedure for the evaluation of mode shapes.

These studies have shown that fairly accurate estimates of the natural frequency can be generally achieved. In contrast to the considerable volume of recent scientific literature on bridge frequency evaluation, only a few studies focus on the indirect identification of modal damping ratios of structures. In this regard, it is pointed out that the vast majority of the aforementioned studies neglect the effect of vehicle damping on the modal identification of the structure, both in the theoretical formulation and/or numerical applications [7,25,26,28,29]. Further, these studies often lead to results characterized by a low degree of accuracy, in which quite evident discrepancies may appear. For instance, González et al. [30] introduced a six-step procedure for modal damping ratio identification where, however, a reduced accuracy of the algorithm has been observed for shorter spans and stiffer structures. Recently, Yang et al. [27] proposed a trial-and-error approach for the estimation of bridge modal damping ratios concurrently to mode shapes using a single-axle scanning vehicle. Notably, however, the analysis is conducted adopting in the theoretical formulation the assumptions of undamped test vehicle and smooth bridge surface. Further, in [31] an identification approach that combines VMD, Random Decrement Technique (RDT) and Hilbert spectrum (HS) analysis is introduced for the estimations of both natural frequencies and damping ratios assuming a single-axle vehicle model. In this case, however, non-negligible discrepancies from theoretical values in damping ratios estimation have been observed increasing the roughness level assumed in the simulations. In this context, it is worth highlighting how modal damping ratios are crucial for accurate identification of the mode shapes. This is due to the vehicle-induced scaling and shifting effects on the mode shapes that can be overcome by a modal damping ratio-based correction [32]. Similarly, it is noted that mode shapes identification via VSM in the presence of road pavement roughness rarely provides reliable estimates if a single-axis test vehicle is adopted. However, enhanced performances can be achieved for instance if a series of connected instrumented vehicles is used in the testing [29].

Based on the preceding conspectus, it is evident that further investigation is required for the development of more suitable procedures potentially improving the identification of modal damping ratios in the context of VSM with a single-axis vehicle.

To this aim, in this paper, an enhanced VMD-based procedure is introduced for accurate modal identification of bridges by exploiting a single-axis vehicle. Specifically, IMFs and corresponding central frequencies are determined by applying the VMD to the recorded signals. Further, the Natural Excitation Technique (NExT) [33,34] in conjunction with an area ratio-based approach is employed for damping ratios assessment and mode shapes estimation, as it will be clarified in Section 3.

In the framework of the existent scientific literature on this topic, the main novel contributions to the proposed procedure are listed as follows:

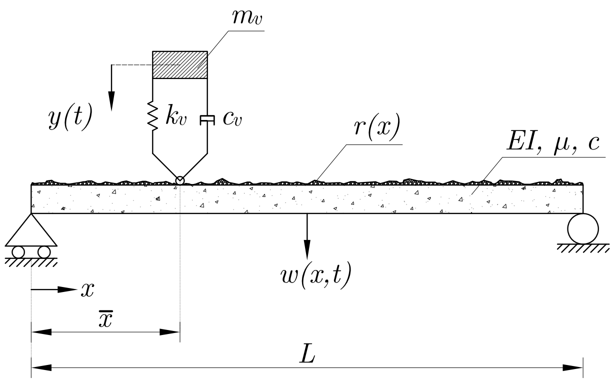

Fig. 1. Schematic of a SDOF moving oscillator (vehicle) crossing a simply supported beam (bridge).

- a comprehensive theoretical formulation taking into account both the vehicle/bridge damping and the road roughness and their separate and concurrent effects on the dynamics of the vehicle–bridge system with specific reference to the performance on the identification of all the modal parameters;
- a more accurate procedure using the NExT approach for the conversion of the extracted IMFs via the VMD to free-vibration-like signals in place of the standard Random Decrement Technique;
- the introduction of a noise-robust area ratio-based approach which yields more accurate and reliable results for the determination of modal damping ratios, which are indeed fundamental also for the subsequent estimations of the mode shapes.

In passing, it is pointed out that both NExT and the noise-robust area ratio-based approach have been previously used in classical direct structural identification purposes. Nevertheless, to the best of the authors' knowledge, their applicability in the context of VSM for indirect dynamic identification has not been documented in the literature so far.

The accuracy of the proposed approach is then assessed via several numerical applications, considering the effect of both vehicle damping and pavement roughness that, as previously mentioned, are rarely considered in the analysis. Finally, the higher accuracy and reliability of the proposed enhanced approach are assessed performing a comparative analysis with an existent reference standard single-axis VSM approach based on HS analysis, which is, to the authors' best knowledge, among the most recent methods considering the application of a VMD-based framework in the case of a single-axle test vehicle.

2. Theoretical formulation

2.1. Vehicle–bridge dynamics

For mathematical description purposes, the vehicle–bridge interaction problem is treated by adopting a well-established simplified model which consists of a simply supported Euler–Bernoulli beam (bridge girder) and a Single-Degree-Of-Freedom (SDOF) oscillator (vehicle) moving over the beam with constant velocity v. The simply-supported beam (see Fig. 1) has span length L, constant bending stiffness EI, mass per-unit-length μ and damping c. The actual road pavement effect is considered by the definition of a roughness profile $r(x)$ with variable amplitude along the span length, superimposed on the beam smooth surface. The equation of motion for the beam can be therefore written as [35]

$$EI\,w''''(x,t) + \mu\ddot{w}(x,t) + c\dot{w}(x,t) = f(x,t) \tag{1}$$

where $w(x,t)$ is the beam vertical displacement while $f(x,t)$ is the interaction force between the moving oscillator and the beam at the contact point. Further, note that in Eq. (1) the over-dot and the prime over a variable indicate the partial derivatives with respect to time t and abscissa x, respectively.

The moving oscillator is described as a discrete mass–spring–damper system with mass m_v, spring stiffness k_v and damping coefficient c_v, which takes into account the effect of vehicle real suspension system. Under the assumption that the SDOF oscillator crosses the beam with constant velocity v, and taking into account the derivations reported in Appendix A, its vertical motion is described by the following equation

$$m_v\ddot{y}(t) + c_v(\dot{y}(t) + \dot{w}(\bar{x},t) + vr'(\bar{x})) + k_v(y(t) - w(\bar{x},t) + r(\bar{x})) = 0 \tag{2}$$

where $y(t)$ is the absolute vertical displacement of the oscillator with respect to the static equilibrium position $y_s = m_v g/k_v$ and $r(\bar{x})$ is the amplitude of the roughness profile evaluated at the contact point position $\bar{x}$. In this manner, the contact force $f(x,t)$ between the oscillator and the bridge may be expressed as follows

$$f(x,t) = [m_v g - c_v(\dot{y}(t) + \dot{w}(\bar{x},t) + vr'(\bar{x})) - k_v(y(t) - w(\bar{x},t) + r(\bar{x}))]\chi(t)\delta(x-\bar{x}) \tag{3}$$

where $\delta(x-\bar{x})$ is the Dirac's delta function centered at the contact point $\bar{x}$ and $\chi(t)$ is the window function defined as

$$\chi(t)=\begin{cases}1 & \text{for } 0\le t\le L/v\\ 0 & \text{otherwise}\end{cases} \tag{4}$$

By combining Eqs. (2) and (3) the contact force may be expressed in the following compact form

$$f(x,t)=\left[m_v g-m_v\ddot{y}(t)\right]\chi(t)\delta(x-\bar{x}) \tag{5}$$

Next, using standard modal superposition approach [36], the beam vertical displacement $w(x,t)$ is approximated as the sum of its first N modes (see Appendix A):

$$w(x,t)\simeq\sum_{k=1}^{N}q_k(t)\phi_k(x) \tag{6}$$

where the equation of motion in terms of the kth modal displacement $q_k(t)$ is given as [37]

$$\ddot{q}_k(t)+2\xi_k\omega_k\dot{q}_k(t)+\omega_k^2 q_k(t)=\varepsilon\chi(t)\phi_k(\bar{x})[g-\ddot{y}(t)] \tag{7}$$

in which $\phi_k(x)$ is the kth mode shape function of the beam and $\varepsilon=m_v/(\mu L)$.

Similarly, the equation of motion of the oscillator can be expressed as

$$\ddot{y}(t)+2\xi_v\omega_v\dot{y}(t)+\omega_v^2 y(t)=2\xi_v\omega_v\left[\sum_{k=1}^{N}\dot{q}_k(t)\phi_k(\bar{x})+v\sum_{k=1}^{N}q_k(t)\phi_k'(\bar{x})-vr'(\bar{x})\right]+\omega_v^2\left[\sum_{k=1}^{N}q_k(t)\phi_k(\bar{x})-r(\bar{x})\right] \tag{8}$$

where $\xi_v=c_v/(2m_v\omega_v)$ is the vehicle damping ratio and $\omega_v^2=k_v/m_v$ is the circular frequency of the vehicle.

It is pointed out that Eqs. (7) and (8) constitute a system of $N+1$ coupled differential equations which governs the dynamic response of the considered system, taking into account the damping in both the bridge and the vehicle, as well as the effect of the road pavement roughness.

2.2. Contact point response estimation

Indirect dynamic identification approaches are usually carried out by elaborating the data recorded by sensors directly mounted on the vehicle body or its axle. However, several studies in the literature [28,38] have shown that the vehicle frequency may significantly affect the recording spectra, overshadowing higher bridge modes, thus limiting the identification to the first structural mode at most. To overcome this limitation, Yang et al. [28] suggested the use of the contact point (CP) response as a more suitable function for dynamic identification purposes. Specifically, considering Eq. (6) the CP displacement $d_{\mathrm{CP}}(t)$ can be expressed as

$$d_{\mathrm{CP}}(t)=w(\bar{x},t)=\sum_{k=1}^{N}q_k(t)\phi_k(\bar{x}) \tag{9}$$

Differentiating twice Eq. (9) with respect to time, the CP acceleration $a_{\mathrm{CP}}(t)$ is obtained as

$$a_{\mathrm{CP}}(t)=\ddot{w}(\bar{x},t)=\sum_{k=1}^{N}(\ddot{q}_k(t)\phi_k(\bar{x})+2v\dot{q}_k(t)\phi_k'(\bar{x})+v^2 q_k(t)\phi_k''(\bar{x})) \tag{10}$$

Notably, the CP acceleration is generally adopted in the dynamic identification procedures, due to the higher magnitude of frequency peaks in the Fourier domain in comparison to the other CP response functions. Clearly, however, the contact response cannot be easily measured in practical applications and, therefore, has to be estimated based on the recorded vehicle vertical acceleration $\ddot{y}(t)$. In this regard, it is possible to back-calculate the CP acceleration exploiting the dynamic vertical equilibrium equation of the vehicle once its acceleration $\ddot{y}(t)$ is known [39] as

$$a_{\mathrm{CP}}(t)=\frac{1}{2\xi_v\omega_v}e^{-\frac{\omega_v}{2\xi_v}t}\int_0^t F(\tau)e^{\frac{\omega_v}{2\xi_v}\tau}d\tau \tag{11}$$

where it is assumed that

$$F(t)=\frac{d^2\ddot{y}(t)}{dt^2}+2\xi_v\omega_v\frac{d\ddot{y}(t)}{dt}+\omega_v^2\ddot{y}(t) \tag{12}$$

In experimental applications, the surface on which the vehicle moves is always not smooth and the recorded vehicle acceleration $\ddot{y}(t)$ implicitly takes into account the effect of surface roughness, thus Eq. (11) can be efficiently adopted to determine the CP acceleration. However, when calculating the CP acceleration in the numerical simulations, Eq. (11) must be appropriately modified considering the explicit effect of the roughness profile $r(x)$. Specifically, differentiating twice Eq. (2) with respect to time, the following differential equation is obtained

$$2\xi_v\omega_v\frac{d\ddot{w}(\bar{x},t)}{dt}+\omega_v^2\ddot{w}(\bar{x},t)=\frac{d^2\ddot{y}(t)}{dt^2}+2\xi_v\omega_v\frac{d^2\dot{y}(t)}{dt^2}+\omega_v^2\frac{d^2y(t)}{dt^2}+2\xi_v\omega_v v^3 r'''(\bar{x})+\omega_v^2 v^2 r''(\bar{x}) \tag{13}$$

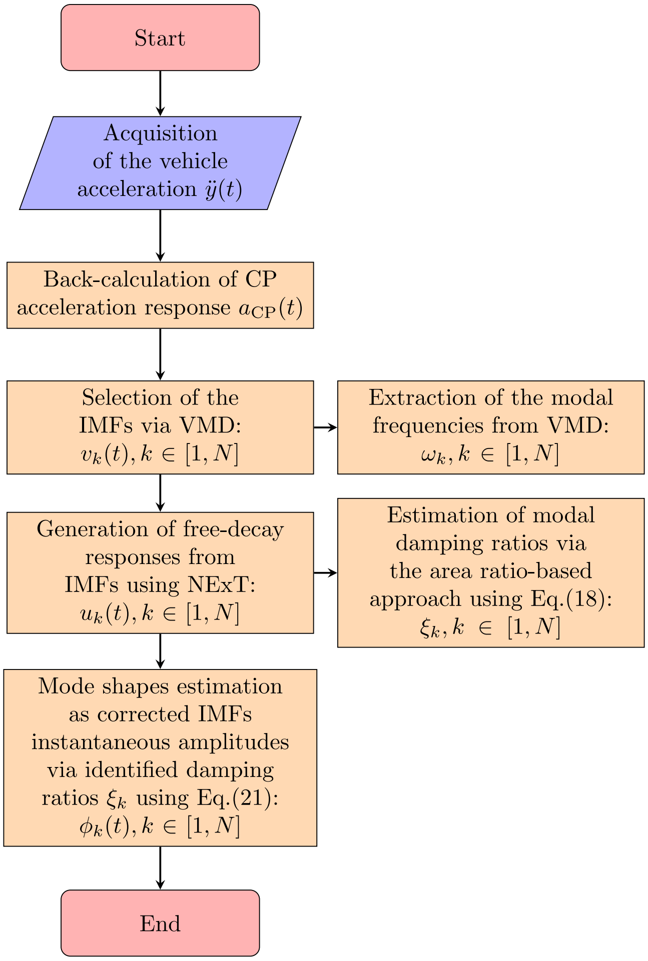

Fig. 2. Flowchart of the proposed modal identification procedure.

which, assuming $\ddot{w}(\bar{x}, t)|_{t=0} = 0$, has the following solution

$$a_{\mathrm{CP}}(t) = \ddot{w}(\bar{x}, t) = \frac{1}{2\xi_v\omega_v} e^{-\frac{\omega_v}{2\xi_v}t} \int_0^t F^*(\tau) e^{\frac{\omega_v}{2\xi_v}\tau} d\tau \tag{14}$$

where

$$F^*(t) = \frac{d^2\ddot{y}(t)}{dt^2} + 2\xi_v\omega_v \frac{d\ddot{y}(t)}{dt} + \omega_v^2\ddot{y}(t) + 2\xi_v\omega_v v^3 r'''(\bar{x}) + \omega_v^2 v^2 r''(\bar{x}) \tag{15}$$

3. Proposed modal identification procedure

In this section, an enhanced modal identification procedure is introduced based on the use of vehicle indirect measurements. The technique can be regarded as an extension of techniques commonly adopted in classical direct identification to the case of indirect modal identification. Specifically, the VMD technique [22] is applied on the contact point response function to estimate the IMFs, and the associated central frequencies, directly retrieved by the decomposition procedure, are assumed as the sought modal frequencies. Each IMF is then converted into a free-decay vibration signal using NExT [33]. Further, the procedure involves proceeding to estimate pertinent modal damping ratios from these signals by employing an appropriately developed noise-robust area ratio-based approach. Finally, mode shapes are captured by using the instantaneous amplitudes of the IMFs, appropriately corrected to account for the influence of the modal damping ratios. The flowchart in Fig. 2 schematically summarizes the aforementioned identification procedure.

3.1. Variational Mode decomposition

The Variational Mode decomposition [22] is an adaptive decomposition technique that allows to extract from an input signal $v(t)$ a set of N amplitude–frequency-modulated functions $v_k(t)$, generally referred to as Intrinsic Mode Functions (IMFs). These functions are characterized by a limited bandwidth and a central pulsation ω_k ($k = 1, \dots, N$) around which the modes frequency content is concentrated. The method consists of: (i) evaluation of the analytical signal for each mode by means of Hilbert–Huang transform [16]; (ii) shift of the spectra to baseband; (iii) estimation of the bandwidth computing the H_1 Gaussian smoothness of demodulated signals. The previous steps lead to the following constrained variational problem

$$\min_{\substack{v_1(t),\dots,v_N(t)\\ \omega_1,\dots,\omega_N}} \left\{ \sum_{k=1}^{N} \left\| \partial_t \left[\left(\delta(t) + \frac{\mathrm{j}}{\pi t} \right) * v_k(t) \right] e^{-\mathrm{j}\omega_k t} \right\|_2^2 \right\} \quad \text{s.t.} \quad \sum_{k=1}^{N} v_k(t) = v(t) \tag{16}$$

where j is the imaginary unit, the symbol "$*$" is the convolution operator, ∂_t is the gradient operator and stands for $\|\cdot\|_2$ the L^2-norm operator. Different methods can be used to solve the optimization problem in Eq. (16). For instance, by using a quadratic penalty term and the Lagrange multipliers technique to enforce the constraints, the following augmented Lagrangian function can be written

$$\begin{aligned} \mathcal{L}(v_1(t), \dots, v_N(t),\ \omega_1 \dots \omega_N, \lambda) =& \alpha \sum_{k=1}^{N} \left\| \partial_t \left[\left(\delta(t) + \frac{\mathrm{j}}{\pi t} \right) * v_k(t) \right] e^{-\mathrm{j}\omega_k t} \right\|_2^2 \\ &+ \left\| v(t) - \sum_{k=1}^{N} v_k(t) \right\|_2^2 + \left\langle \lambda, v(t) - \sum_{k=1}^{N} v_k(t) \right\rangle \end{aligned} \tag{17}$$

where α is the quadratic penalty factor, λ is the Lagrangian multiplier and $\langle \cdot \rangle$ is the L^2-inner product. The solution of the governing constrained problem is thus equivalent to the evaluation of the saddle point of the augmented Lagrangian function. Therefore, the solution of the problem defined by Eq. (17), namely the set of IMFs $v_k(t)$ and central frequencies ω_k ($k = 1, \dots, N$) is obtained through an iteration updating process in the frequency domain exploiting the Alternating Direction Method of Multipliers (ADMM). Further details on the resolution procedure may be found in [22]. The extracted $v_k(t)$ component corresponds to the contribution to the response of the kth mode of vibration, whereas ω_k is the estimate of the associated natural frequency.

3.2. Area ratio-based approach for modal damping ratio estimation

Once each IMF $v_k(t)$ is retrieved by means of the VMD, it is possible to associate the corresponding free-decay response, hereinafter labeled as $u_k(t)$, exploiting the NExT properties [33,34]. Specifically, this method allows to generate impulse-like response functions for the analyzed system, based on measured structural responses to white noise excitation. The generated free-decay functions are therefore exploited for the evaluation of the modal damping ratios ξ_k following an approach based on the evaluation of the areas under the system time history response, as originally formulated for a single-degree-of-freedom (SDOF) system by Huang et al. [40]. The main advantage of this approach consists in a strong anti-noise property which leads to more accurate damping estimations. Notably, real signals are always affected to a certain noise degree which cannot be completely removed even using filtering procedures; this, in turn, may produce significant distortions near the local maxima of the response. Traditional damping estimation techniques such as the logarithmic decrement method or curve fitting procedures, which exploit response peaks, may thus suffer from this problem leading to inaccurate estimations. On the other hand, the area ratio-based approach mitigates the noise effect because the evaluation of the areas is significantly less affected by the response local distortions, thus allowing more accurate damping estimations.

This methodology proved to be effective in direct identification problems as in Mazzeo et al. [24], where the modal damping ratios in existing bridges have been identified exploiting free vibration responses recorded by sensors directly attached to the structure. This study aims to extend the aforementioned procedure to vehicle scanning indirect identification problems under ambient excitation and prove its reliability.

In this regard, consider that the kth free-decay response function $u_k(t)$, associated with the kth mode, has $2S_k + 1$ zero-crossing points and, consequently, $2S_k$ areas are enclosed between the former and the time axis, namely $A_{1,k}, \dots, A_{2S,k}$ (see Fig. 3). It can be proved that the damping ratio corresponding to the kth mode has the following expression

$$\xi_k = \frac{1}{\sqrt{1 + \left(2S_k\pi / r_k\right)^2}} \tag{18}$$

where

$$r_k = \ln\left[\frac{\sum_{i=1}^{S_k} A_{i,k}}{\sum_{i=S_k+1}^{2S_k} A_{i,k}} \right] \tag{19}$$

The ratio r_k may be calculated using any quadrature method for the estimation of $A_{i,k}$. This procedure is therefore repeated for all the selected modes, i.e. for each $u_k(t)$ with $k \in [1, N]$, to complete the damping ratios identification process.

3.3. Mode shapes estimation

Once the IMFs $v_k(t)$ and damping ratios ξ_k have been evaluated, a procedure may be followed to estimate mode shapes, appropriately extending an approach firstly introduced in [41]. Specifically, by applying the Hilbert transform operator to each IMF $v_k(t)$, the associated signal can be defined as:

$$\tilde{v}_k(t) = v_k(t) + \mathrm{j}\mathcal{H}[v_k(t)] = \bar{A}_k(t) e^{\mathrm{j}\theta(t)} \quad \text{with} \quad k \in [1, N] \tag{20}$$

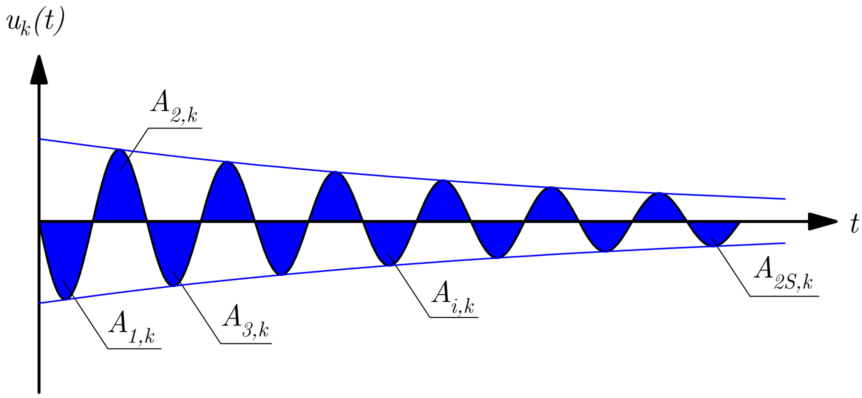

Fig. 3. Schematic of the areas enclosed by the kth free-decay modal response function $u_k(t)$ extracted via NExT.

where $\mathcal{H}[\cdot]$ is the Hilbert transform operator, $\bar{A}_k(t)$ is the instantaneous amplitude function associated with the kth IMF and $\theta(t)$ the corresponding instantaneous phase.

As shown in [41], the instantaneous amplitude function $\bar{A}_k(t)$ which is, by the Hilbert transform properties, the envelope of $v_k(t)$, may represent a first estimate, in absolute value, of the corresponding mode shape function associated with the instantaneous frequency ω_k.

On the other hand, as discussed in [32], the bridge damping ratios effect produces a combined shifting and scaling of the IMFs instantaneous amplitude if compared with the undamped case.

However, it is possible to account for the damping ratio effect on each mode shape estimation by properly correcting it as in [32]. Thus, the estimated mode shapes (in absolute value) can be given as

$$\phi_k(x) = \frac{\bar{A}_k\,(x/v)}{e^{-\xi_k \omega_k x/v}} \quad \text{with} \quad k \in [1, N] \tag{21}$$

Notably, the estimated mode shapes according to Eq. (21), should be normalized with respect to their corresponding maximum to be compared with their theoretical counterpart.

4. Numerical applications

In this section the proposed dynamic identification procedure is validated on numerical applications, investigating the effects of vehicle damping ratio and pavement roughness. Modal frequencies and damping ratios, determined according to the above-mentioned procedure, are compared to the estimates obtained by the Hilbert Spectrum (HS) based approach, whose theoretical formulation is reported in Appendix B. Further, the performance of the proposed area-ratio based approach for modal damping ratios estimation is discussed by comparing two different free vibration response extraction procedures, namely NExT and RDT, to show the superiority of the former over the latter in this task.

In this regard, note that the numerical applications presented in the following are based on a vehicle–bridge system whose properties are listed in Table 1.

4.1. Case 1: Vehicle-bridge system neglecting vehicle damping and road pavement roughness

The first numerical application deals with the most simple-vehicle bridge system; that is a sprung mass moving at a constant velocity v on a simply supported Euler–Bernoulli beam. Further, both the effects of the vehicle damping ξ_v and pavement roughness are neglected ($\xi_v = 0$, $r(x) = 0$), while the bridge damping ratio ξ_k with $k \in [1, N]$ is assumed constant for each mode. Note that a small velocity value in the simulations is employed to avoid the so-called camel hump effect [42], i.e. the splitting in the frequency spectrum of higher modes frequencies into left and right shifted components.

In this regard, the equations of motion (7) and (8) are solved, evaluating the bridge and vehicle responses in terms of displacement, velocity and acceleration (see Figs. 4(a)–(f)). Next, using the approach described in Section 2.2, the contact point response function in terms of displacement, velocity and acceleration, and the corresponding frequency spectra, are determined (see Figs. 5).

As it can be seen in Figs. 5(a)–(c), the proposed indirect approach (red line) yields response functions that perfectly match those obtained using classical modal superposition (blue dashed line), thus underlining the reliability of the back-calculation method. Moreover, it is observed that the contact point acceleration (see Fig. 5(f)) is the most suitable response function for indirect dynamic identification purposes due to the highest level of peaks amplitude found for higher modes in comparison with the CP displacement and CP velocity functions (see Figs. 5(d) and 5(e)). Therefore, hereinafter the CP acceleration is chosen for the application of the proposed dynamic identification approach. In this manner, applying the VMD procedure, the first four IMFs (see Figs. 6(a)–(d)) have

Table 1
Properties for the investigated vehicle–bridge system.

Bridge			
Young's modulus	E	$2.8 \cdot 10^{10}$	[N/m^2]
Moment of inertia	I	0.2	[m^4]
Mass-per-unit-length	μ	5400	[kg/m]
Length	L	30	[m]
Modal circular frequency	ω_1	1.78	[Hz]
	ω_2	7.11	[Hz]
	ω_3	16.00	[Hz]
	ω_4	28.44	[Hz]
Modal damping ratio (equal for all the modes)	ξ_k	2	[%]
Vehicle			
Mass	m_v	1000	[kg]
Spring stiffness	k_v	$8 \cdot 10^5$	[N/m]
Velocity	v	4	[m/s]
Circular frequency	ω_v	4.50	[Hz]
Damping ratio	ξ_v	5	[%]

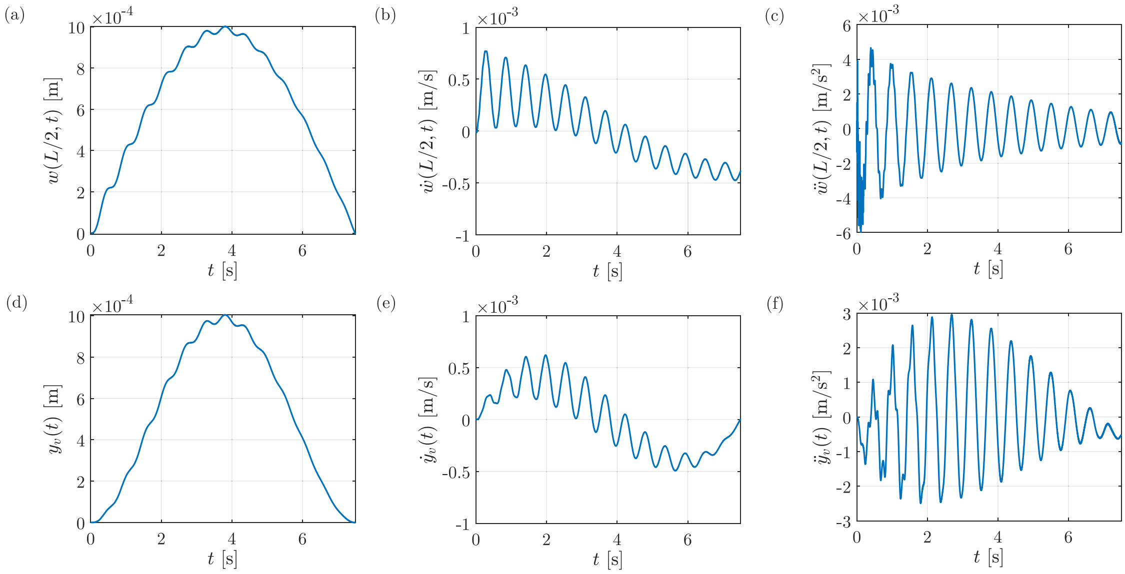

Fig. 4. Displacement, velocity and acceleration time-histories for the vehicle–bridge system in Fig. 1 neglecting the vehicle damping and road pavement roughness ($\xi_v = 0$, $r(x) = 0$): (a) bridge response displacement, (b) velocity and (c) acceleration at midspan; (d) vehicle response displacement, (e) velocity and (f) acceleration.

been identified, whereas the vehicle frequency was neither observable in the frequency spectrum nor retrieved in the decomposition process. The identified modal frequencies obtained via VMD are listed in Table 2.

The free vibrations associated with the IMFs have been extracted by means of both NExT and RDT. For further comparison, the natural frequencies have been also estimated from the free vibrations using the HS approach. The identified frequencies obtained with the different approaches and their corresponding relative errors are summarized in Table 2. It is observed that the estimated frequencies obtained as VMD central frequencies are overall the most accurate ones with errors of less than 1%.

Similarly, a comparison between damping ratios estimates is carried out as shown in Table 3. Specifically, for the free-decay functions extracted via NExT and RDT, both the area-ratio based approach and the HS one are considered. As it can be seen, for the free vibrations functions extracted by both NExT and RDT, the proposed area-ratio based approach is preferable, leading to significantly lower errors (less than 5%) in comparison to the HS-based approach.

Finally, the first two mode shapes of the examined system have been correctly identified through the proposed approach while higher modes have not been estimated satisfactorily due to the lower level of excitation obtainable in indirect identification approaches. Notably, Figs. 7(a) and 7(b) show that estimated mode shapes are in good agreement with the theoretical counterparts. However, it is also observed a sharp edge effect in both Figs. 7, which accentuates as the bridge damping ratios increase: this, in turn, has a detrimental impact on the exploited technique accuracy in constructing mode shapes. In this regard, a jump in each mode shape function is expected due to the edge effect generated by the damping ratio-based correction in Eq. (21). Specifically, the higher the modal damping ratio, the stronger the edge effect will be. This phenomenon depends on the fact that the final part of

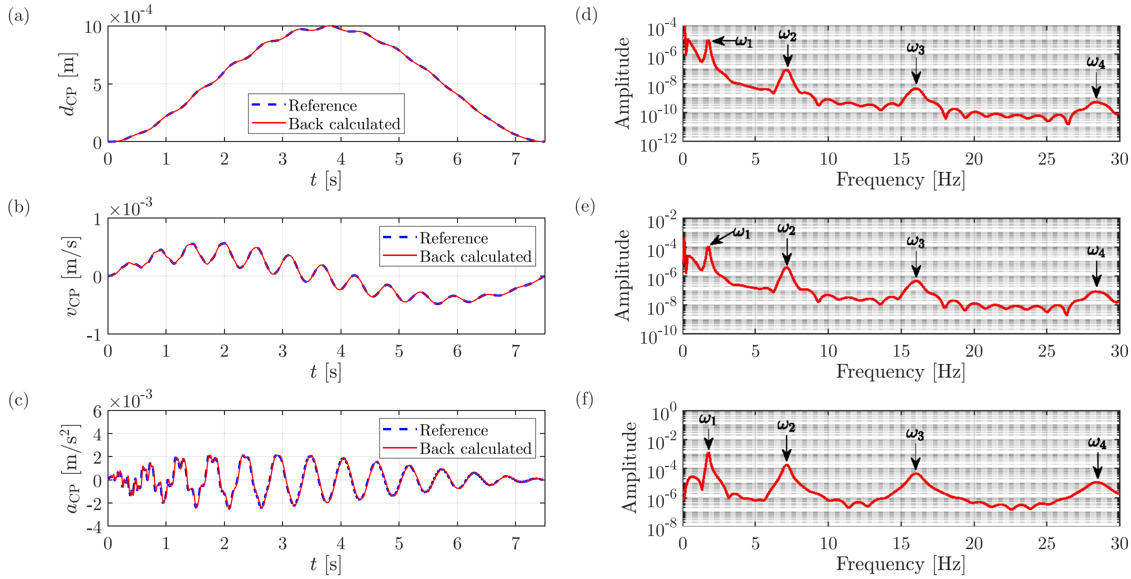

Fig. 5. Reference and back-calculated CP response functions (from (a) to (c)) and corresponding frequency spectra (from (d) to (f)) for the vehicle–bridge system in Fig. 1 neglecting vehicle damping and road pavement roughness ($\xi_v = 0$, $r(x) = 0$): CP displacement (top), CP velocity (middle) and CP acceleration (bottom).

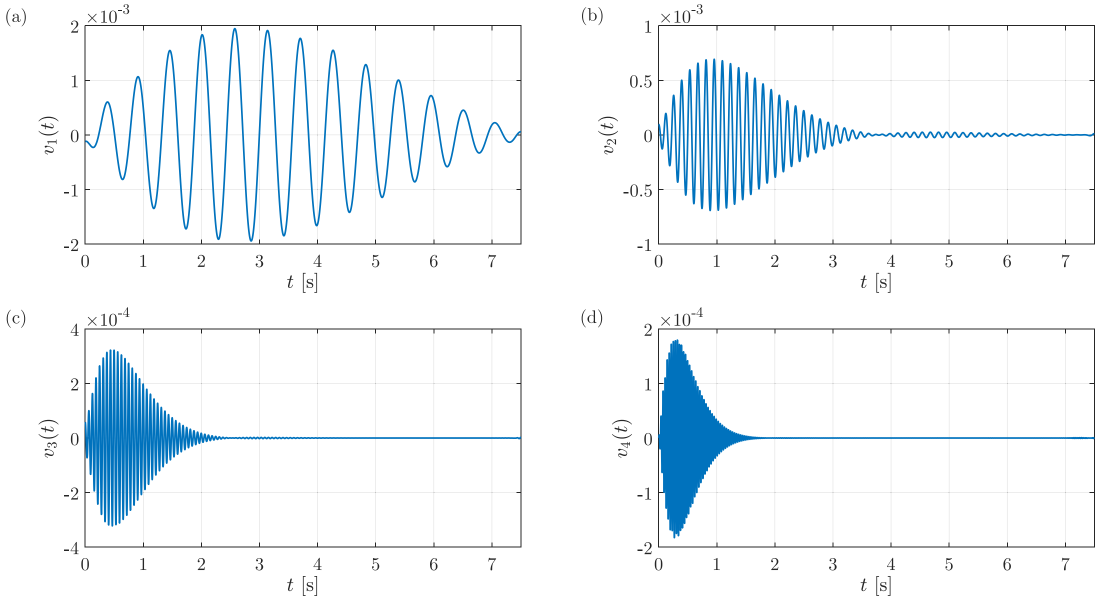

Fig. 6. IMFs extracted via the VMD from the CP acceleration of the vehicle–bridge system in Fig. 1 neglecting vehicle damping and road pavement roughness ($\xi_v = 0$, $r(x) = 0$): (a) first IMF, (b) second IMF, (c) third IMF and (d) fourth IMF.

each estimated instantaneous amplitude signal is not smooth enough and the mode shape correction process amplifies this feature. A possible solution to this issue can be pursued by a preventive smoothing of the instantaneous amplitude signals before employing Eq. (21).

4.2. Case 2: Vehicle–bridge system considering vehicle damping and neglecting road pavement roughness

In the present application, the same vehicle–bridge system properties of the previous case are adopted. However, since vehicle damping cannot be usually neglected when considering the features of the testing vehicle due to the actual suspensions system, a reasonable damping ratio value, i.e. $\xi_v = 5\%$, is here adopted following other literature studies [43]. For this case study the road pavement roughness is still neglected ($r(x) = 0$). As in the previous case, for dynamic identification purposes, the CP acceleration is

Table 2
Identification of the bridge natural frequencies from the vehicle–bridge system in Fig. 1 assuming $\xi_v = 0$ and $r(x) = 0$. Comparison of the proposed method with Hilbert spectrum-based approach. The absolute value of relative error is given within brackets.

Mode number	Theoretical [Hz]	Identified frequencies [Hz]	
		Proposed VMD	Hilbert spectrum based approach
1	1.777	1.782 (0.26%)	1.783 (0.36%)
2	7.109	7.147 (0.51%)	7.152 (0.53%)
3	15.996	16.023 (0.17%)	15.94 (0.33%)
4	28.438	28.479 (0.15%)	28.283 (0.54%)

Table 3
Identification of bridge damping ratios from the vehicle–bridge system in Fig. 1 assuming $\xi_v = 0$ and $r(x) = 0$. Comparison of the proposed method, using alternatively NExT and RDT, with Hilbert spectrum-based approach. The absolute value of relative error is given within brackets.

Mode number	Theoretical [%]	Identified damping ratios [%]		
		Area-ratio based approach		Hilbert spectrum based approach
		NExT	RDT	
1	2	2.06 (2.94%)	2.01 (0.64%)	2.79 (39.35%)
2	2	2.04 (1.95%)	2.10 (4.91%)	2.42 (20.88%)
3	2	2.03 (1.28%)	2.06 (2.85%)	2.10 (5.17%)
4	2	2.02 (1.00%)	2.02 (0.98%)	2.05 (2.71%)

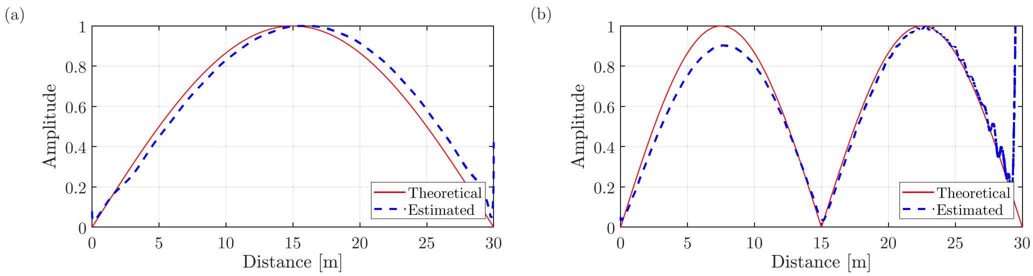

Fig. 7. Comparison between theoretical and estimated mode shapes for (a) the first and (b) second mode for the vehicle–bridge system in Fig. 1 neglecting vehicle damping and road pavement roughness ($\xi_v = 0, r(x) = 0$).

Table 4
Identification of bridge natural frequencies from the vehicle–bridge system in Fig. 1 assuming $\xi_v = 5\%$ and $r(x) = 0$. Comparison of the proposed method with Hilbert spectrum-based approach. The absolute value of relative error is given within brackets.

Mode number	Theoretical [Hz]	Identified frequencies [Hz]	
		Proposed VMD	Hilbert spectrum based approach
1	1.777	1.782 (0.27%)	1.782 (0.28%)
2	7.109	7.147 (0.53%)	7.153 (0.609%)
3	15.996	16.023 (0.17%)	15.943 (0.33%)
4	28.437	28.479 (0.15%)	28.285 (0.54%)

here employed (see Figs. 8(a) and 8(b)). It is observed that the vehicle damping effect slightly alters the CP acceleration response amplitude as well as the peaks magnitude of the frequency spectrum in comparison with the previous case. However, for dynamic identification purposes, no significant alterations have been shown and the first four modes have been accurately determined. The proposed identification procedure has been therefore applied to the extracted mode functions leading to the estimations of modal frequencies (see Table 4) and damping ratios (see Table 5). It may be observed that the slight variations in CP response and its corresponding frequency spectrum are reflected on the estimated modal parameters which show, in general, small discrepancies compared to the results in Section 4.1. Further, it is also observed that damping ratios estimates with all the examined procedures are more sensitive to this effect than the natural frequencies. Notably, again the proposed area ratio-based approach leads to the most accurate results. Similarly to the previous case, the first two mode shapes have been reliably evaluated and compared with theoretical previsions (see Figs. 9(a) and 9(b)). Further, comparing these results with Figs. 7(a) and 7(b), slight variations in estimated mode shapes can be observed, proving that a higher accuracy can be reached in appraisals if the vehicle damping is taken into account.

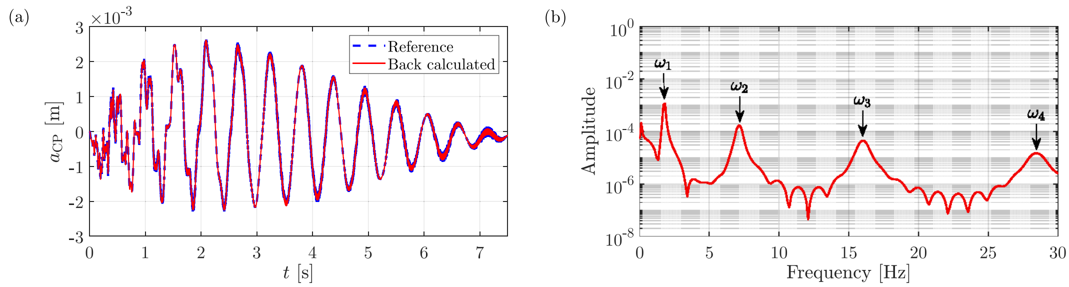

Fig. 8. (a) Reference and back-calculated contact point acceleration and (b) corresponding frequency spectrum for the vehicle–bridge system in Fig. 1 in presence of vehicle damping $\xi_v = 5\%$, and neglecting road pavement roughness ($r(x) = 0$).

Table 5
Identification of bridge damping ratios from the vehicle–bridge system in Fig. 1 assuming $\xi_v = 5\%$, and $r(x) = 0$. Comparison of the proposed method, using alternatively NExT and RDT, with Hilbert spectrum-based approach. The absolute value of relative error is given within brackets.

Mode number	Theoretical [%]	Identified damping ratios [%]		
		Area-ratio based approach		Hilbert spectrum based approach
		NExT	RDT	
1	2	2.06 (3.06%)	1.89 (5.65%)	2.54 (27.33%)
2	2	2.08 (4.31%)	2.07 (3.78%)	2.56 (28.44%)
3	2	2.04 (2.33%)	2.01 (0.12%)	2.35 (17.56%)
4	2	2.03 (1.84%)	1.98 (0.72%)	2.09 (4.341%)

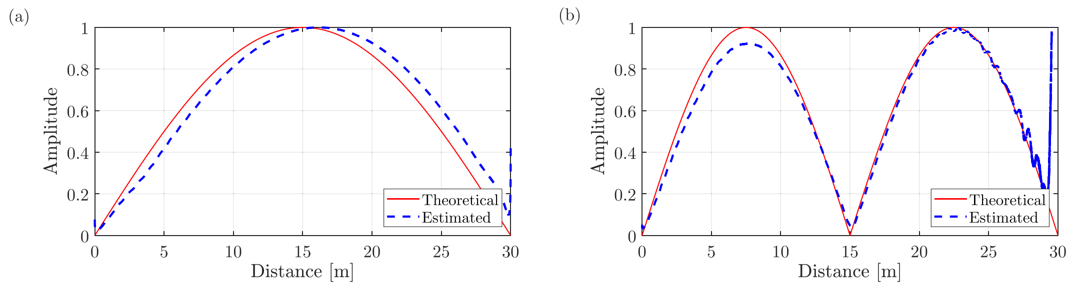

Fig. 9. Comparison between theoretical and estimated mode shapes for (a) the first and (b) second mode for the vehicle–bridge system in Fig. 1 assuming $\xi_v = 5\%$ and $r(x) = 0$.

4.3. Case 3: Vehicle–bridge system considering road pavement roughness and neglecting vehicle damping

In this section, the vehicle damping is neglected ($\xi_v = 0$) whereas the effect of pavement roughness ($r(x) \neq 0$) is investigated on the vehicle–bridge system responses and the performance of the proposed modal identification procedure is assessed. The construction of the longitudinal road profile can be carried out by exploiting a set of harmonic waves with different amplitudes and phases. The road profile is therefore generated by its spectral description according to the method proposed by Shinozuka et al. [44,45]; the one-sided PSD spectrum is discretized in bands and for each one of them a fixed number of harmonic samples is generated assuming a uniformly distributed random phase angle θ_i:

$$r(x) = \sum_{i=0}^{N^*} \sqrt{2G_d(n_i)\Delta n}\cos(2\pi n_i + \theta_i) \tag{22}$$

where N^* is the number of harmonics chosen to simulate the profile, n_i is the ith spatial frequency, Δn is the sampling interval of the spatial frequency and θ_i is the random phase angle for the ith harmonic. A possible formulation for the PSD function $G_d(n_i)$ is the one proposed in the ISO 8608 standard [46] as

$$G_d(n_i) = G_d(n_0)\left(\frac{n_i}{n_0}\right)^w \tag{23}$$

where $w = 2$ is a waviness coefficient, $n_0 = 0.1$ cycle/m is the reference spatial frequency, $G_d(n_0)$ is the PSD function value at the reference spatial frequency and n_i is the ith spatial frequency calculated as $n_i = n_l + (i - 0.5)\Delta n$ with $\Delta n = (n_u - n_l)/N^*$, being n_u and n_l the spatial frequency upper and lower bounds. On this base, different roughness classes can be defined, depending on the surface quality, by properly selecting the PSD value $G_d(n_0)$, where higher values correspond to worse pavement roughness conditions.

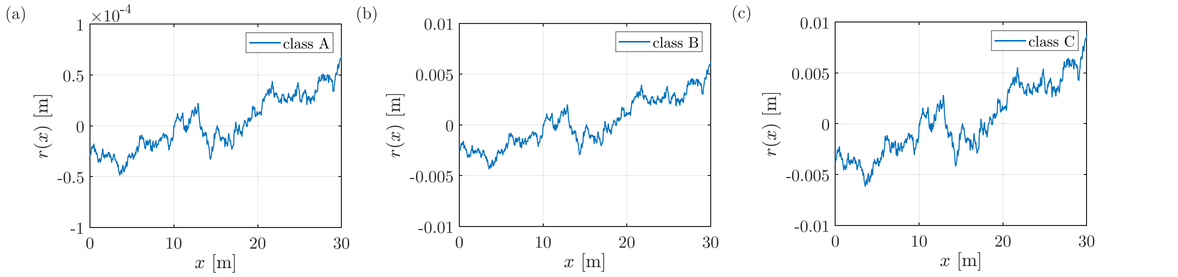

Fig. 10. Different classes of roughness profiles generated according to ISO 8608 with corrected PSD reference values according to [47]: (a) class A - $G_d^*(n_0) = 0.001 \cdot 10^{-6}$ m^3; (b) class B - $G_d^*(n_0) = 8 \cdot 10^{-6}$ m^3; (c) class C - $G_d^*(n_0) = 16 \cdot 10^{-6}$ m^3.

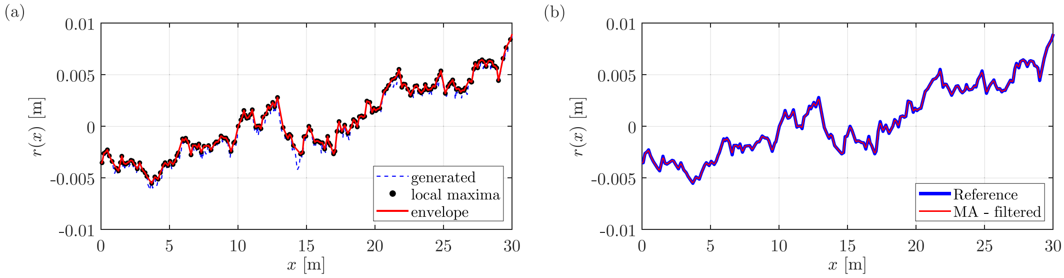

Fig. 11. Class C roughness profile generation: (a) construction of the envelope of local maximum points and (b) profile smoothing via moving average filtering.

In that regard the PSD function values proposed in ISO 8608 were derived from data collected on roads: it is neither considered that bridge pavements are usually in much better conditions than road ones nor that this model was developed for transportation engineering applications rather than for vehicle indirect dynamic identification. For these reasons, the PSD function value at the reference spatial frequency $G_d(n_0)$ is properly corrected from the geometric mean provided by ISO 8608 as described in [47] and is therein labeled as $G_d^*(n_0)$. Specifically, three roughness classes are considered assuming three different values of $G_d(n_0)$ to simulate different surface quality, namely $G_d^*(n_0) = 0.001 \cdot 10^{-6}$ m^3 (class A), $G_d^*(n_0) = 8 \cdot 10^{-6}$ m^3 (class B) and $G_d^*(n_0) = 16 \cdot 10^{-6}$ m^3 (class C). The roughness profiles adopted in this study are generated assuming $N^* = 2500$, $n_u = 10$ cycles/m, $n_l = 0.01$ cycles/m, and samples of the generated profiles are shown in Figs. 10(a)–(c). In passing, it is pointed out that in this study different levels of road roughness are considered, in agreement with the classification proposed by the ISO standards, to show how the influence of this parameter is reflected in the performance of the proposed method.

The contact point response is highly sensitive to the irregularities in the pavement and the use of the generated road profiles leads to highly noisy results. However the tyre, during the passage on the pavement, touches only the point of the surface with higher elevation [12] and the real vehicle–bridge contact is a surface rather than a point. Thus, a moving average filter may be used to smooth the profile [39] and in place of the roughness profile, the smoothed envelope of its local maxima is employed (see Figs. 11(a) and 11(b)).

Figs. 12(a)–(d) show the system response functions considering the highest level of roughness: it is observed that the effect of roughness significantly affects the theoretical response functions of both vehicle and bridge if compared to Figs. 4(a)–(f). Further, Figs. 13(a)–(f) show the CP responses and their corresponding frequency spectrum considering the roughness profile effect. In this regard, it may be observed that also in this scenario it is preferable to choose the CP acceleration response for identification purposes. As opposed to the previous cases, considering the roughness effect on the CP response, the vehicle frequency appears with significant magnitude in the frequency spectrum. This, however, does not preclude the identification of the first few structural frequencies, which are still easily distinguishable. Further, Figs. 14(a)–(f) show how the CP acceleration and the corresponding frequency spectrum change as the roughness class varies. It is observed that, increasing the value of $G_d^*(n_0)$, a wide range of spatial frequencies at increasing magnitudes is introduced in the CP spectrum, thus overshadowing higher order modes (e.g., the fourth mode cannot be detected when higher roughness classes profiles are considered). Next, applying the proposed VMD, up to four modes have been identified when a Class A roughness profile has been adopted and up to three in the remaining cases. As an example of the decomposition results, Figs. 15(a)–(c) show the three IMFs extracted for class C roughness. The application of the proposed procedure led to the natural frequencies and damping ratio estimates summarized in Tables 6 and 7. Notably, again the natural frequency estimations obtained via the proposed VMD are in general more accurate than the counterpart estimated via the HS approach, with relative errors in most of the cases less than 1%, regardless of the adopted roughness class profile. Further, it may be noted how, for the damping ratios estimation, the area ratio-based approach yields significantly better results compared to the HS-based approach independently of the technique adopted for the free vibration extraction from the IMFs. This depends on the fact that the area ratio-based approach is a robust method against noise as observed in Section 3.2. In particular, it is noted

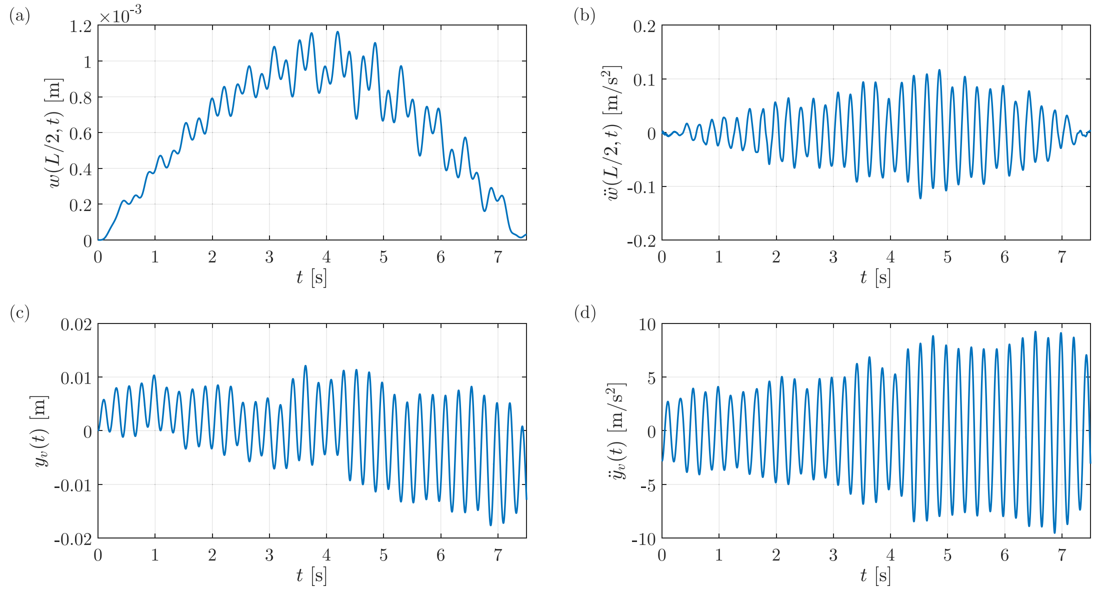

Fig. 12. Displacement and acceleration time–history for the vehicle–bridge system in Fig. 1 neglecting the vehicle's damping ($\xi_v = 0$) and considering a class C road pavement roughness profile: (a) bridge response displacement and (b) acceleration at midspan; (c) vehicle response displacement and (d) acceleration.

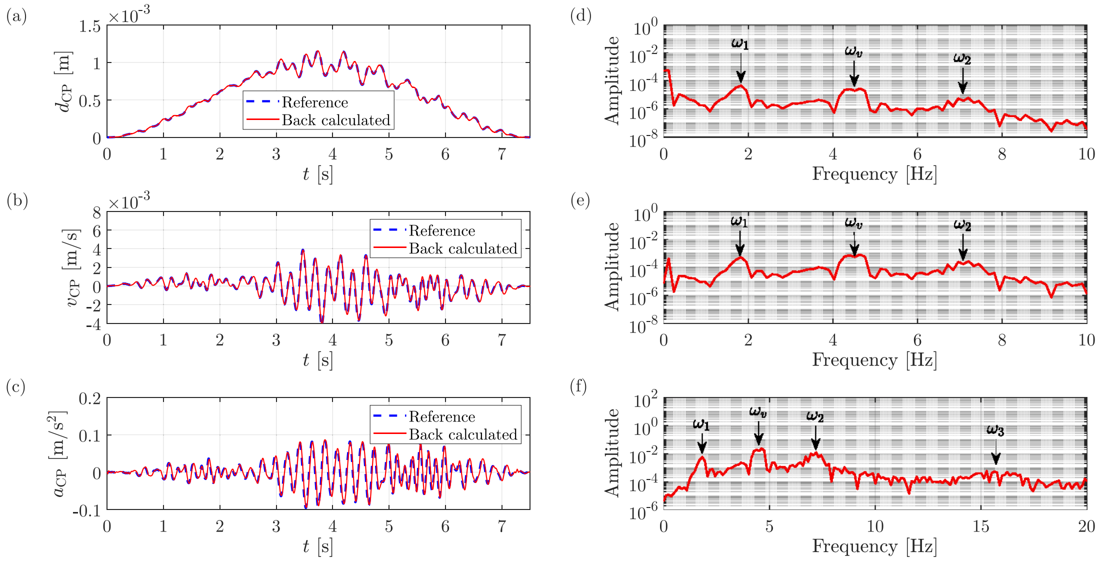

Fig. 13. Reference and back-calculated contact point response functions (form (a) to (c)) and corresponding frequency spectra (from (d) to (f)) considering the vehicle–bridge system in Fig. 1 neglecting the vehicle's damping ($\xi_v = 0$) and considering a class C road pavement roughness profile: CP displacement (top), CP velocity (middle) and CP acceleration (bottom).

that the combination of NExT and area-ratio based approach yields the most precise estimates. It is also observed that the quality of estimations for both natural frequencies and damping ratios tends to get worse for increasing roughness classes.

Further, Fig. 16(a) shows the estimated mode shape for the first mode considering the Class A roughness profile. It is noted, however, that for higher roughness and higher modes, unreliable mode shapes estimations have been obtained and for this reason not represented in the graphics.

4.4. Case 4: Vehicle-bridge system considering both vehicle damping and road pavement roughness

The last application considered in this study deals with the most general case of vehicle–bridge systems in which neither the vehicle damping nor the road roughness profile is neglected ($\xi_v \neq 0$, $r(x) \neq 0$). The mechanical and geometrical properties are

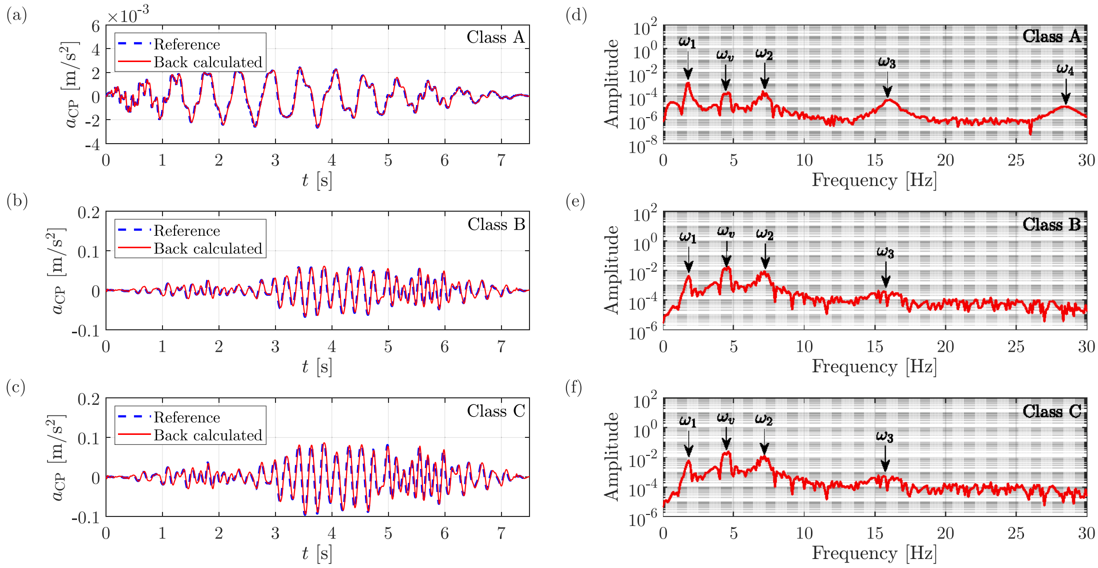

Fig. 14. CP accelerations (from (a) to (c)) and corresponding frequency spectra (from (d) to (f)) for the vehicle–bridge system in Fig. 1 neglecting the vehicle's damping ($\xi_v = 0$) and considering three different roughness classes: Class A (top), Class B (middle) and Class C (bottom).

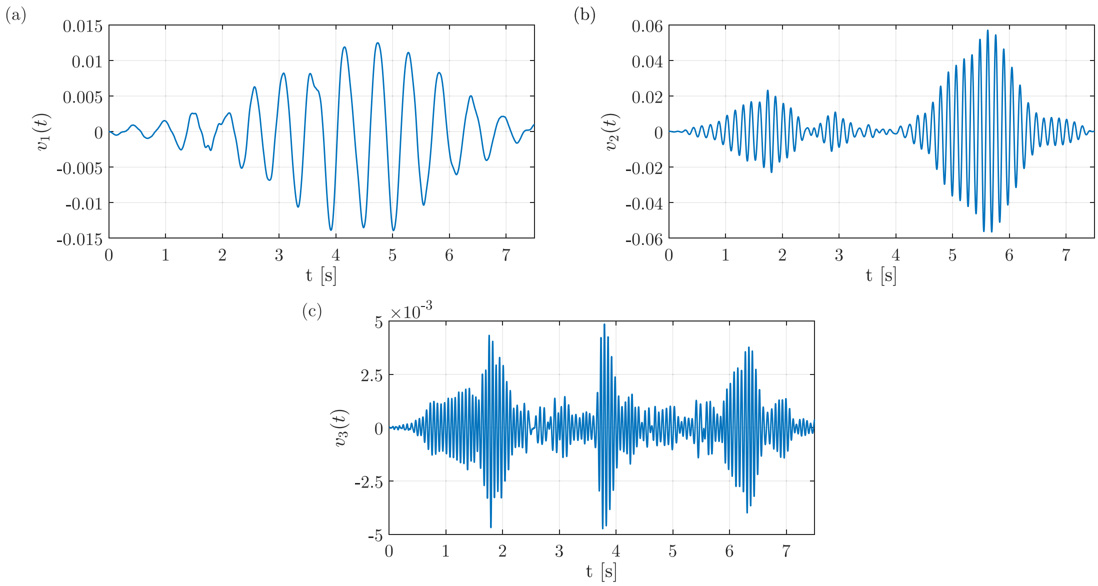

Fig. 15. IMFs extraction via VMD for the analyzed CP acceleration function considering a class C road pavement roughness class: (a) first IMF, (b) second IMF, (c) third IMF.

assumed as in Section 4.1, the vehicle damping ratio is assumed $\xi_v = 5\%$ and the same three roughness class profiles are considered as in Section 4.3. Figs. 17(a)–(f) display the CP acceleration and the corresponding frequency spectrum for different roughness classes.

Even though the CP accelerations present only slight differences in their local response peaks if compared to their counterparts in Figs. 14(a)–(f), the main differences are observed in the frequency spectra since the magnitude of the peak frequency related to the vehicle in the frequency spectrum significantly reduced regardless of the roughness profile class. This result is consistent with the numerical studies conducted by Yang and Lee [48] where it has been shown that the assumption of a high vehicle damping ratio both reduces the surface roughness-related noise and limits the vehicle frequency peak.

The application of the proposed procedure leads to the identification of the first four modes for a Class A roughness profile, whereas for higher roughness classes the fourth mode was overshadowed and only the first three have been retrieved. Tables 8 and 9 summarize the identified natural frequencies and damping ratios, respectively, for each corresponding roughness class. It is

Table 6
Identification of bridge natural frequencies from the vehicle–bridge system in Fig. 1 assuming different classes of road pavement roughness and $\xi_v = 0$. Comparison of the proposed method with Hilbert spectrum-based approach. The absolute value of relative error is given within brackets.

Roughness class	Mode number	Theoretical [Hz]	Identified frequencies [Hz]	
			Proposed VMD	Hilbert spectrum based approach
A	1	1.777	1.782 (0.245%)	1.775 (0.13%)
	2	7.109	6.795 (4.42%)	7.117 (0.10%)
	3	15.996	16.028 (0.20%)	16.053 (0.35%)
	4	28.437	28.45 (0.06%)	28.316 (0.43%)
B	1	1.777	1.867 (5.04%)	1.794 (0.96%)
	2	7.109	7.147 (0.53%)	7.185 (1.06%)
	3	15.996	15.916 (0.50%)	16.840 (5.26%)
C	1	1.777	1.863 (4.84%)	1.817 (2.21%)
	2	7.109	7.145 (0.50%)	7.134 (0.34%)
	3	15.996	15.913 (0.52%)	16.84 (5.26%)

Table 7
Identification of bridge damping ratios from the vehicle–bridge system in Fig. 1 assuming different classes of road pavement roughness and $\xi_v = 0$. Comparison of the proposed method, using alternatively NExT and RDT, with Hilbert spectrum-based approach. The absolute value of relative error is given within brackets.

Roughness class	Mode number	Theoretical [%]	Identified damping ratios [%]		
			Area-ratio based approach		Hilbert spectrum based approach
			NExT	RDT	
A	1	2	2.13 (6.34%)	1.94 (2.95%)	2.65 (32.52%)
	2	2	1.97 (1.31%)	1.73 (13.43%)	1.73 (13.66%)
	3	2	1.93 (3.30%)	2.08 (4.44%)	2.33 (16.39%)
	4	2	1.96 (1.84%)	1.94 (2.94%)	2.14 (7.28%)
B	1	2	2.19 (9.75%)	3.11 (55.99%)	2.96 (48.06%)
	2	2	2.11 (5.43%)	2.41 (20.49%)	2.76 (38.03%)
	3	2	2.65 (32.94%)	1.83 (8.67%)	4.00 (100.20%)
C	1	2	2.23 (11.57%)	3.93 (96.78%)	4.70 (137.01%)
	2	2	2.11 (5.60%)	2.38 (19.13%)	3.08 (54.40%)
	3	2	2.65 (32.69%)	1.85 (7.23%)	3.98 (98.88%)

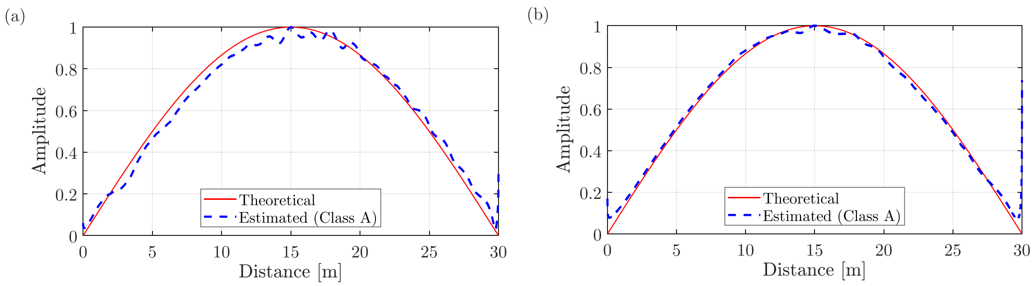

Fig. 16. Comparison between theoretical and estimated mode shapes for the first mode for the vehicle–bridge system in Fig. 1 assuming a Class A road pavement roughness and: (a) $\xi_v = 0\%$, (b) $\xi_v = 5\%$.

noted that, consistently with the results of the previous cases, the proposed procedure provides the most accurate estimates. It is also consistently observed that the quality of the estimates tends to worsen as the roughness class increases due to the rising level of noise introduced in the CP response-related frequency spectrum. Once again, a reliable estimation of the first mode shape has been obtained and compared with the theoretical counterpart (see Fig. 16(b)). Further, from the comparison with Fig. 16(a) it is noted that, for fixed roughness class, the effect of vehicle damping mitigates its detrimental effect improving the precision of the estimated mode shape.

5. Conclusions

In this paper, an enhanced indirect modal identification procedure has been introduced in the context of the so-called Vehicle Scanning Method. Specifically, the contact-point (CP) acceleration function, determined via an approximate closed-form solution of the equations of motion, has been adopted for the identification scheme. In this regard, the Intrinsic Mode Functions (IMFs) have

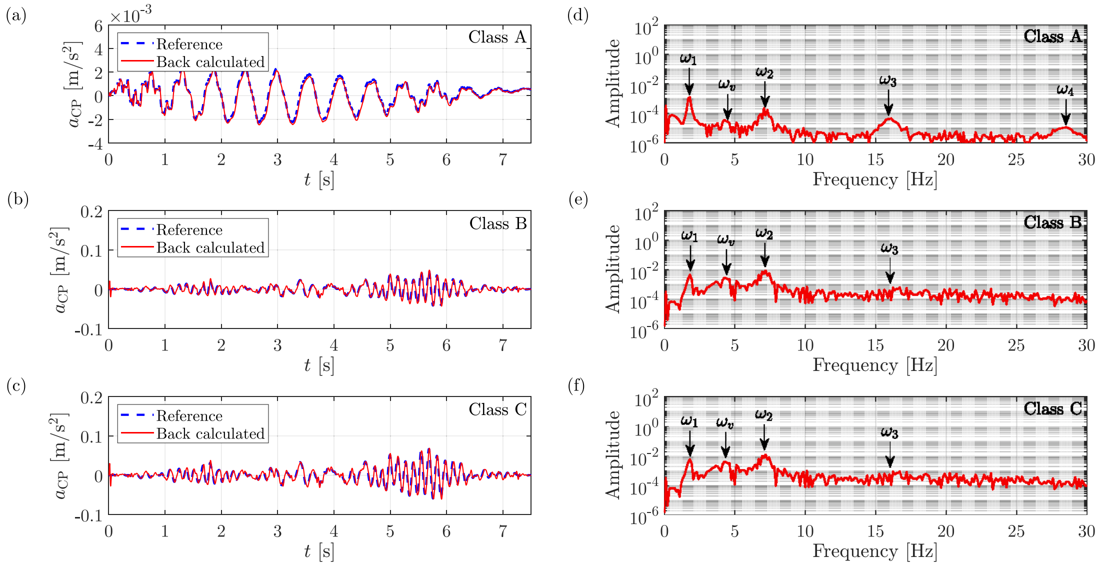

Fig. 17. CP accelerations (from (a) to (c)) and corresponding frequency spectra (from (d) to (f)) for the vehicle–bridge system in Fig. 1 assuming $\xi_v = 5\%$ and considering different roughness classes: Class A (top), Class B (middle) and Class C (bottom).

Table 8
Identification of bridge natural frequencies from the vehicle–bridge system in Fig. 1 assuming $\xi_v = 5\%$ and different classes of road pavement roughness. Comparison of the proposed method with Hilbert spectrum-based approach. The absolute value of relative error is given within brackets.

Roughness class	Mode number	Theoretical [Hz]	Identified frequencies [Hz]	
			Proposed VMD	Hilbert spectrum based approach
A	1	1.777	1.784 (0.38%)	1.780 (0.19%)
	2	7.109	7.150 (0.56%)	7.129 (0.27%)
	3	15.996	16.029 (0.20%)	16.136 (0.87%)
	4	28.437	28.404 (0.12%)	28.24 (0.69%)
B	1	1.777	1.868 (5.09%)	1.818 (2.32%)
	2	7.109	7.139 (0.41%)	7.163 (0.75%)
	3	15.996	15.949 (0.30%)	16.864 (5.42%)
C	1	1.777	1.877 (5.63%)	1.787 (0.54%)
	2	7.109	7.139 (0.41%)	7.147 (0.53%)
	3	15.996	15.934 (0.39%)	16.96 (6.05%)

Table 9
Identification of bridge damping ratios from the vehicle–bridge system in Fig. 1 assuming $\xi_v = 5\%$ and different classes of road pavement roughness. Comparison of the proposed method, using alternatively NExT and RDT, with Hilbert spectrum-based approach. The absolute value of relative error is given within brackets.

Roughness class	Mode number	Theoretical [%]	Identified damping ratios [%]		
			Area-ratio based approach		Hilbert spectrum based approach
			NExT	RDT	
A	1	2	1.90 (5.24%)	1.83 (8.35%)	3.71 (85.39%)
	2	2	1.82 (8.78%)	1.96 (2.24%)	2.17 (8.53%)
	3	2	1.94 (3.21%)	1.98 (0.93%)	1.91 (4.46%)
	4	2	2.00 (0.24%)	2.03 (1.82%)	2.14 (7.19%)
B	1	2	2.17 (8.73%)	2.10 (5.15%)	1.42 (28.78%)
	2	2	2.03 (1.52%)	2.69 (34.50%)	2.87 (43.38%)
	3	2	2.48 (24.08%)	2.03 (1.52%)	3.91 (95.80%)
C	1	2	2.19 (9.99%)	2.52 (26.13%)	3.44 (71.87%)
	2	2	2.03 (1.40%)	2.18 (9.34%)	3.24 (62.22%)
	3	2	2.62 (31.23%)	2.24 (12.01%)	1.79 (10.54%)

been determined from the CP acceleration response through the Variational Mode Decomposition (VMD) and the corresponding central frequencies, given by the decomposition procedure, have been adopted as modal frequencies. Further, the modal damping ratios have been estimated by employing the Natural Excitation Technique (NExT), used to convert the IMFs into free-decay responses, in conjunction with a noise-robust area ratio-based approach. Finally, mode shapes have been evaluated from the IMF instantaneous amplitude functions appropriately accounting for the effect of the estimated modal damping ratios. Several numerical applications have been discussed to assess the performance of this method, comparing NExT and Random Decrement Technique (RDT) for the generation of the free-decay responses, and the proposed technique with a Hilbert spectrum-based approach for the estimation of modal frequencies and damping ratios. In passing, it is pointed out that in real applications, the main challenges are posed by vehicle damping and pavement roughness. In this regard, to appropriately account for their detrimental effects, their roles have been thoroughly investigated in the CP response functions, thus assessing the applicability of the proposed approach in real conditions. Notably, this aspect is often omitted in a relevant number of studies. Specifically, the contemporary effect of these parameters is usually neglected in the theoretical formulation, as well as in numerical applications in the literature, whereas the present study has highlighted the relevance of the influence of the road roughness profile and the vehicle damping both in terms of system response and modal identification.

In this regard, three different pavement roughness profiles have been considered, showing how the accuracy of the identification procedure decreases as the roughness class increases. Furthermore, results have emphasized the positive influence of vehicle damping, which yields a reduction of the overshadowing effect due to the vehicle frequency on higher modes in the frequency domain, regardless of the pavement road roughness. Notably, all the numerical applications have shown that the proposed identification method leads to increased accuracy in the estimations of the sought modal parameters compared to standard approaches. Specifically, analyses have pointed out how the area ratio-based approach represents an accurate and robust method for the modal damping ratios estimation, thus proving the overall reliability and enhanced performance of the developed identification framework. Finally, despite the presence of possible edge effects, comparisons of the identified mode shapes vis-à-vis theoretical results have shown a satisfactory level of accuracy. In this regard, again it can be noted how vehicle damping improves mode shapes estimations, even though the overall precision decreases as the road roughness level increases.

CRediT authorship contribution statement

Matteo Mazzeo: Writing – review & editing, Writing – original draft, Methodology, Investigation, Formal analysis, Data curation, Conceptualization. **Alberto Di Matteo:** Writing – review & editing, Writing – original draft, Validation, Methodology, Investigation, Formal analysis, Data curation, Conceptualization. **Roberta Santoro:** Writing – review & editing, Writing – original draft, Validation, Supervision, Methodology, Investigation, Formal analysis, Data curation, Conceptualization.

Declaration of competing interest

The authors declare that they have no known competing financial interests or personal relationships that could have appeared to influence the work reported in this paper.

Data availability

Data will be made available on request.

Appendix A. Equation of motion derivation for SDOF moving oscillator

Consider the system represented in Fig. 18. Let it be $y_s = m_v g/k_v$ the static vertical displacement of the SDOF oscillator due to its weight, $y_v(t)$ its relative vertical displacement inclusive of the static contribution, $w(\bar{x},t)$ the contact point displacement, $y(t)$ its absolute displacement, $\bar{y}(t)$ the corresponding absolute displacement inclusive of the static contribution and $r(x)$ the road pavement roughness profile.

It is possible to relate the relative vertical displacements and the corresponding absolute displacements via the following relations

$$y_v(t) = y(t) - w(\bar{x},t) + r(\bar{x}) + y_s; \qquad y(t) = \bar{y}(t) - y_s \tag{A.1}$$

Therefore, the following relation holds

$$y_v(t) = \bar{y}(t) - w(\bar{x},t) + r(\bar{x}) \tag{A.2}$$

From the equilibrium of forces applied to the oscillator, the equation of motion takes the following expression

$$m_v \ddot{\bar{y}}(t) + c_v \dot{y}_v(t) + k_v y_v(t) = m_v g \tag{A.3}$$

The derivative $\dot{y}_v(t)$ may be expressed as follows

$$\dot{y}_v(t) = \frac{d}{dt}(y(t) - w(\bar{x},t) + r(\bar{x}) + y_s) = \dot{y}(t) - \dot{w}(\bar{x},t) + v r'(\bar{x}) \tag{A.4}$$

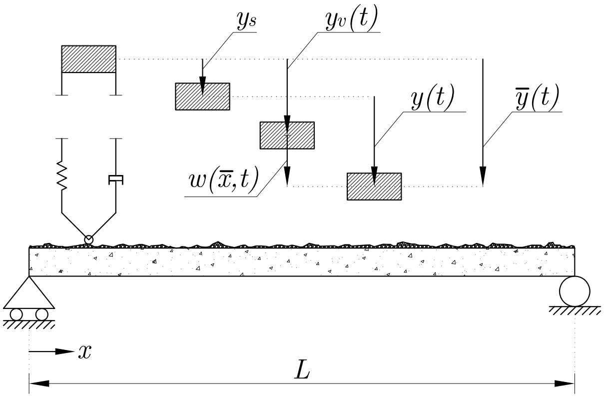

Fig. 18. Displacements of a SDOF moving oscillator crossing a simply supported beam.

Considering that $\ddot{\bar{y}}(t) = \ddot{y}(t)$ and substituting Eq. (A.4) into Eq. (A.3) the equation of motion of the oscillator becomes

$$m_v\ddot{y}(t) + c_v(\dot{y}(t) + \dot{w}(\bar{x},t) - vw'(\bar{x},t) + vr'(\bar{x})) + k_v(y(t) - w(\bar{x},t) + r(\bar{x})) = 0 \tag{A.5}$$

The modal superposition principle used to approximate the beam vertical displacement $w(x,t)$ as the sum of its first N modes reads:

$$w(x,t) \simeq \sum_{k=1}^{N} q_k(t)\phi_k(x) \tag{A.6}$$

The mode shape functions $\phi_k(x)$ with $k \in [1,N]$ are obtained from the solution of the following eigenproblem

$$\phi_k''''(x) = \lambda_k^4\phi_k(x) \text{ with } k \in [1,N] \tag{A.7}$$

where $\lambda_k^4 = \mu\omega_k^2/EI$, and ω_k is the circular frequency for the kth mode. Further, considering the orthogonality conditions

$$\int_0^L \phi_k(x)\phi_j(x)dx = 0 \quad \forall k \neq j \tag{A.8}$$

substituting Eq. (6) into Eq. (1), pre-multiplying both sides by $\phi_j(x)$, and integrating with respect to x over the length of the beam L, the equations of motion of the beam in modal coordinates are

$$\ddot{q}_k(t) + 2\xi_k\omega_k\dot{q}_k(t) + \omega_k^2 q_k(t) = \chi(t)\frac{\phi_k(\bar{x})}{\mu\int_0^L \phi_k^2(x)dx}[m_v g - m_v\ddot{y}(t)] \quad \forall k \in [1,N] \tag{A.9}$$

Assuming as normalization condition $\int_0^L \phi_k^2(x)dx = L$, Eq. (7) is obtained. Similarly, substituting Eq. (6) into Eq. (2) and dividing by the mass m_v, Eq. (8) is obtained.

Appendix B. Hilbert spectrum-based identification

Let $u_k(t)$ be the kth free-decay response associated with the kth mode function extracted via VMD. By applying the Hilbert transform the associated analytic signal is

$$u_k^{\mathrm{A}} = u_k(t) + \mathrm{j}\mathcal{H}[u_k(t)] = a_k(t)e^{\mathrm{j}\psi_k(t)} \tag{B.1}$$

where $\mathcal{H}[\cdot]$ is the Hilbert transform operator, $a_k(t)$ and $\psi_k(t)$ denote the kth instantaneous amplitude and phase angle, respectively. It is possible to show that the kth modal damped frequency, may be obtained as

$$\omega_{d,k} = \frac{d\psi_k(t)}{dt} \tag{B.2}$$

and geometrically it represents the slope of the phase angle $\psi_k(t)$ versus time t plot. Furthermore, the value $-\xi_k\omega_{n,k}$ may be obtained as the slope of the decaying amplitude $\ln a_k(t)$ versus time t plot. Using the linear least-square method, the above-mentioned slopes can be computed as parameters that define the corresponding fitting curves. Therefore, the kth natural frequency $\omega_{n,k}$ and damping ratio ξ_k may be evaluated as

$$\omega_{n,k} = \sqrt{s_{\psi,k}^2 + s_{a,k}^2}; \qquad \xi_k = \sqrt{\frac{s_{a,k}^2}{s_{\psi,k}^2 + s_{a,k}^2}} \tag{B.3}$$

where $s_{\psi,k}$ and $s_{a,k}$ are the slopes of the phase angle $\psi_k(t)$ and decaying amplitude $\ln a_k(t)$ versus time plot, respectively.

References

[1] M. Gul, F.N. Catbas, Ambient vibration data analysis for structural identification and global condition assessment, J. Eng. Mech. 134 (8) (2008) 650–662.
[2] B. Gunes, O. Gunes, Vibration-based damage evaluation of a reinforced concrete frame subjected to cyclic pushover testing, Shock Vib. 2021 (2021) 1–16.
[3] Y.-B. Yang, J.P. Yang, Y. Wu, B. Zhang, Vehicle Scanning Method for Bridges, John Wiley & Sons, 2019.
[4] Y.-B. Yang, C. Lin, J. Yau, Extracting bridge frequencies from the dynamic response of a passing vehicle, J. Sound Vib. 272 (3–5) (2004) 471–493.
[5] Y. Yang, C. Lin, Vehicle–bridge interaction dynamics and potential applications, J. Sound Vib. 284 (1–2) (2005) 205–226.
[6] Y. Yang, B. Zhang, T. Wang, H. Xu, Y. Wu, Two-axle test vehicle for bridges: Theory and applications, Int. J. Mech. Sci. 152 (2019) 51–62.
[7] D. Cantero, P. McGetrick, C.-W. Kim, E. OBrien, Experimental monitoring of bridge frequency evolution during the passage of vehicles with different suspension properties, Eng. Struct. 187 (2019) 209–219.
[8] C. Lin, Y. Yang, Use of a passing vehicle to scan the fundamental bridge frequencies: An experimental verification, Eng. Struct. 27 (13) (2005) 1865–1878.
[9] A. Di Matteo, D. Fiandaca, A. Pirrotta, Smartphone-based bridge monitoring through vehicle–bridge interaction: analysis and experimental assessment, J. Civ. Struct. Health Monit. 12 (6) (2022) 1329–1342.
[10] D. Fiandaca, A. Di Matteo, B. Patella, N. Moukri, R. Inguanta, D. Llort, A. Mulone, A. Mulone, S. Alsamahi, A. Pirrotta, An integrated approach for structural health monitoring and damage detection of bridges: An experimental assessment, Appl. Sci. 12 (24) (2022) 13018.
[11] S. Laflamme, F. Ubertini, A. Di Matteo, A. Pirrotta, M. Perry, Y. Fu, J. Li, H. Wang, T. Hoang, B. Glisic, et al., Roadmap on measurement technologies for next generation structural health monitoring systems, Meas. Sci. Technol. (2023).
[12] R. Corbally, A. Malekjafarian, Examining changes in bridge frequency due to damage using the contact-point response of a passing vehicle, J. Struct. Integr. Maint. 6 (3) (2021) 148–158.
[13] X. Kong, C. Cai, B. Kong, Numerically extracting bridge modal properties from dynamic responses of moving vehicles, J. Eng. Mech. 142 (6) (2016) 04016025.
[14] H. Wang, T. Nagayama, J. Nakasuka, B. Zhao, D. Su, Extraction of bridge fundamental frequency from estimated vehicle excitation through a particle filter approach, J. Sound Vib. 428 (2018) 44–58.
[15] C. Liu, Y. Zhu, H. Ye, Bridge frequency identification based on relative displacement of axle and contact point using tire pressure monitoring, Mech. Syst. Signal Process. 183 (2023) 109613.
[16] N.E. Huang, Z. Shen, S.R. Long, M.C. Wu, H.H. Shih, Q. Zheng, N.-C. Yen, C.C. Tung, H.H. Liu, The empirical mode decomposition and the Hilbert spectrum for nonlinear and non-stationary time series analysis, Philos. Trans. R. Soc. Lond. Ser. A Math. Phys. Eng. Sci. 454 (1971) (1998) 903–995.
[17] Z. Wu, N.E. Huang, Ensemble empirical mode decomposition: a noise-assisted data analysis method, Adv. Adapt. Data Anal. 1 (01) (2009) 1–41.
[18] Y. Yang, K. Chang, Extraction of bridge frequencies from the dynamic response of a passing vehicle enhanced by the EMD technique, J. Sound Vib. 322 (4–5) (2009) 718–739.
[19] K. Kildashti, M.M. Alamdari, C. Kim, W. Gao, B. Samali, Drive-by-bridge inspection for damage identification in a cable-stayed bridge: Numerical investigations, Eng. Struct. 223 (2020) 110891.
[20] L. Zhu, A. Malekjafarian, On the use of ensemble empirical mode decomposition for the identification of bridge frequency from the responses measured in a passing vehicle, Infrastructures 4 (2) (2019) 32.
[21] S.S. Eshkevari, T.J. Matarazzo, S.N. Pakzad, Bridge modal identification using acceleration measurements within moving vehicles, Mech. Syst. Signal Process. 141 (2020) 106733.
[22] K. Dragomiretskiy, D. Zosso, Variational mode decomposition, IEEE Trans. Signal Process. 62 (3) (2013) 531–544.
[23] W. Yang, Z. Peng, K. Wei, P. Shi, W. Tian, Superiorities of variational mode decomposition over empirical mode decomposition particularly in time–frequency feature extraction and wind turbine condition monitoring, IET Renew. Power Gener. 11 (4) (2017) 443–452.
[24] M. Mazzeo, D. De Domenico, G. Quaranta, R. Santoro, Automatic modal identification of bridges based on free vibration response and variational mode decomposition technique, Eng. Struct. 280 (2023) 115665.
[25] Y. Yang, H. Xu, X. Mo, Z. Wang, Y. Wu, An effective procedure for extracting the first few bridge frequencies from a test vehicle, Acta Mech. 232 (2021) 1227–1251.
[26] Y. Yang, Y. Liu, H. Xu, Recovering mode shapes of curved bridges by a scanning vehicle, Int. J. Mech. Sci. 253 (2023) 108404.
[27] Y. Yang, Z. Li, Z. Wang, Z. Liu, Z. Zhou, D. Guo, H. Xu, Refining the modal properties of damped bridges scanned by a single-axle test vehicle with field proof, J. Sound Vib. (2023) 117849.
[28] Y. Yang, B. Zhang, Y. Qian, Y. Wu, Contact-point response for modal identification of bridges by a moving test vehicle, Int. J. Struct. Stab. Dyn. 18 (05) (2018) 1850073.
[29] Y. He, J.P. Yang, Z. Yan, Enhanced identification of bridge modal parameters using contact residuals from three-connected vehicles: Theoretical study, in: Structures, vol. 54, Elsevier, 2023, pp. 1320–1335.
[30] A. González, E.J. OBrien, P. McGetrick, Identification of damping in a bridge using a moving instrumented vehicle, J. Sound Vib. 331 (18) (2012) 4115–4131.
[31] Y. Yang, K. Shi, Z. Wang, H. Xu, B. Zhang, Y. Wu, Using a single-DOF test vehicle to simultaneously retrieve the first few frequencies and damping ratios of the bridge, Int. J. Struct. Stab. Dyn. 21 (08) (2021) 2150108.
[32] C. Tan, N. Uddin, E.J. OBrien, P.J. McGetrick, C.-W. Kim, Extraction of bridge modal parameters using passing vehicle response, J. Bridge Eng. 24 (9) (2019) 04019087.
[33] G.H. James III, T.G. Carne, J.P. Lauffer, The Natural Excitation Technique (Next) for Modal Parameter Extraction from Operating Wind Turbines, Tech. Rep., Sandia National Labs., Albuquerque, NM (United States), 1993.
[34] G.H. James, T.G. Carne, J.P. Lauffer, et al., The natural excitation technique (NExT) for modal parameter extraction from operating structures, Modal Anal. - Int. J. Anal. Exp. Modal Anal. 10 (4) (1995) 260.
[35] L. Fryba, Vibration of Solids and Structures Under Moving Loads, Thomas Telford, 1999.
[36] Z.-F. Fu, J. He, Modal Analysis, Elsevier, 2001.
[37] A. Di Matteo, Dynamic response of beams excited by moving oscillators: Approximate analytical solutions for general boundary conditions, Comput. Struct. 280 (2023) 106989.
[38] Y. Yang, J.P. Yang, State-of-the-art review on modal identification and damage detection of bridges by moving test vehicles, Int. J. Struct. Stab. Dyn. 18 (02) (2018) 1850025.
[39] H. Xu, C. Huang, Z. Wang, K. Shi, Y. Wu, Y. Yang, Damped test vehicle for scanning bridge frequencies: Theory, simulation and experiment, J. Sound Vib. 506 (2021) 116155.
[40] F.-L. Huang, X.-M. Wang, Z.-Q. Chen, X.-H. He, Y.-Q. Ni, A new approach to identification of structural damping ratios, J. Sound Vib. 303 (1–2) (2007) 144–153.
[41] Y. Yang, Y. Li, K.C. Chang, et al., Constructing the mode shapes of a bridge from a passing vehicle: a theoretical study, Smart Struct. Syst. 13 (5) (2014) 797–819.
[42] Z. Shi, N. Uddin, Extracting multiple bridge frequencies from test vehicle–a theoretical study, J. Sound Vib. 490 (2021) 115735.
[43] D. Yang, C. Wang, Modal properties identification of damped bridge using improved vehicle scanning method, Eng. Struct. 256 (2022) 114060.

[44] M. Shinozuka, C.-M. Jan, Digital simulation of random processes and its applications, J. Sound Vib. 25 (1) (1972) 111–128.
[45] M. Shinozuka, Monte Carlo solution of structural dynamics, Comput. Struct. 2 (5–6) (1972) 855–874.
[46] ISO 8608:2016 mechanical vibration - road surface profiles - reporting of measured data, 2016, International Organization for Standardization.
[47] Y. Yang, Y. Li, K. Chang, Effect of road surface roughness on the response of a moving vehicle for identification of bridge frequencies, Interact. Multiscale Mech. 5 (4) (2012) 347–368.
[48] J.P. Yang, W.-C. Lee, Damping effect of a passing vehicle for indirectly measuring bridge frequencies by EMD technique, Int. J. Struct. Stab. Dyn. 18 (01) (2018) 1850008.